OPTIMIZED CONFORMAL PARAMETERIZATION WITH CONTROLLABLE AREA DISTORTIONS

KA CHUN LAM AND LOK MING LUI

Abstract. Parameterization, a process of mapping a complicated domain onto a simple canonical domain, is crucial in different areas such as computer graphics, medical imaging and scientific computing. Conformal parameterization has been widely used since it preserves the local geometry well. However, a major drawback is the area distortion introduced by the conformal parameterization, causing inconvenience in many applications such as texture mapping in computer graphics or visualization in medical imaging. This work proposes a remedy to obtain a parameterization that balances between conformality and area distortions. We present a variational algorithm to compute the optimized conformal parameterization with controllable area distortions. The distribution of the area distortion can be prescribed by users according to the application. The main idea is to minimize a combined energy functional involving the Beltrami coefficient and Jacobian of the map, which are used to control the conformality and area distortions respectively. Landmark constraints can be incorporated into the model to obtain landmark-aligned parameterization. Experiments have been carried out on both synthetic and real data. Results demonstrate the efficacy of the proposed model to obtain an optimized parameterization with controllable area distortion while preserving the local geometry as good as possible.

Key words. Area preserving mapping, Beltrami coefficient, conformality distortion, parameterization, texture mapping.

1. Introduction. Surface parameterization of 3D geometric objects has central importance in the field of geometry processing. It refers to the process of mapping a surface one-to-one and onto a simple parameter domain. Applications can be found in various fields such as computer graphics, medical imaging and scientific computing. Recently, various surface parameterization techniques have been introduced.

In general, surface parameterization introduces different kinds of distortions. Depending on applications, different parameterization algorithms aim to minimize different types of distortions. For example, isometric parameterization aims to preserve the metric tensor as good as possible. Authalic projection minimizes the area distortion under the parameterization. Amongst the various parameterization techniques, the conformal parameterization has been extensively used, since it preserves angles and hence the local geometry well. However, a major drawback of the conformal parameterization is that it introduces area distortion. Although angles are preserved, some regions on the surface can be seriously squeezed on the parameter domain. This leads to problems in some practical applications in scientific computing and computer graphics. For instance, in computer graphics, surface conformal parameterizations can be used for texture mapping. The goal is to project a 2D image onto the surface to increase the realism of the 3D model. When there is a huge area distortion under the texture map, the projected texture on the surface may look unnatural. In practice, it is more desirable to obtain a parameterization whose distortions are controllable by users.

In this paper, we propose a variational model to obtain an optimized conformal parameterization with controllable area distortions. Depending on the specific application, the distribution of the area distortion under the conformal parameterization can be prescribed by users. Our goal is to find an optimal map from the surface onto a simple domain, such that the area distortion follows the prescribed distribution as much as possible while minimizing the conformality distortion. The key idea is to minimize a combined energy functional involving the Beltrami coefficient and Jacbobian of the mapping. The Beltrami coefficient term aims to control the confor-

mality distortion and hence the local geometric distortion under the parameterization. The area term involving the Jacobian aims to control the area distortion under the mapping. Parameters in the energy model can be adjusted by users to balance between the conformality and area distortions. Sometimes, landmark features of the surface are required to be projected to desired locations. For this purpose, landmark constraints can also be incorporated in our proposed model. In this work, we propose to apply a splitting method to minimize the proposed energy functional, which alternatively optimizes the energy terms involving the Beltrami coefficient and the mapping respectively. Experiments have been carried out to parameterize different surface models. Results demonstrate the efficacy of our proposed method to obtain an optimized parameterization that preserves both local geometry and area distortion as good as possible. Applications of the proposed parameterization method in computer graphics and medical imaging are also shown.

In short, the contributions of this paper are two-folded. Firstly, we propose a variational model to obtain the optimized conformal parameterization with controlled area distortion. Secondly, we propose to incorporate feature landmarks into the model to obtain meaningful parameterizations with consistent feature alignment.

The rest of the paper is organized as follows. In Section 2, we describe some previous works closely related to our paper. In Section 3, we introduce the basic mathematical concepts about the conformal and quasi-conformal geometry. In Section 3, our proposed parameterization model is described in details. The numerical implementation of the proposed model is explained in Section 4. Experimental results are shown in Section 5. Conclusion and future works are discussed in Section 6.

2. Previous work. In this section, we give an overview of the previous works related to the paper.

2.1. Conformal parameterization. Conformal surface parameterization, which minimizes angular distortions, has been widely used to obtain parameterizations which preserve local geometry well [12, 15, 35, 36]. Least square conformal map (LSCM), which was proposed by Bruno et al. in [27] , and the discrete conformal parameterization proposed by Desbrun et al. in [4] are two well-known variational methods to compute conformal mapping/ parameterization with free boundaries. However, the obtained results obtained are often affected by the quality of the input triangular meshes, due to the use of cotangent formula. Later, Muller et al. [28] proposed the spectral conformal parameterization. The basic idea is to consider the eigenvalue problem of a sparse, symmetric matrix. This provides a convenient and efficient way to find a parameterization that minimizes the conformal energy. However, a folding-free parameterization cannot guaranteed. Haker et al. [11] applied the conformal surface parameterization to obtain angle preserving texture mapping. However, conformal parameterization generally cannot cope with feature correspondence and causes severe area distortion. Gu et al. [10] and Lui et al. [22] proposed the algorithm for finding conformal parameterizations of genus-zero closed surfaces and apply them to landmark-based brain surface registration with optimized conformality distortion. Since gradient descent based algorithms are used, the computation costs of these algorithms are comparitively high. Recently, Choi et al. [3] proposed the FLASH algorithm, which can efficiently parameterize a genus-zero closed surface with prescribed landmark constraints by solving a few linear systems.

2.2. Area preserving parameterization. Several works have been done on flattening surfaces with area preserving constraints [1]. Dominitz et al. applied the

optimal mass transport technique to find the area preserving parameterization, which was used for texture mapping [6]. Zhao et al. [38] improved the efficiency of the optimal mass transport technique to find the area-preserving flattening which is based on the Monge-Brenier theory. Zou et al. [39] proposed to use Lie advection to compute the area preserving surface mapping. However, all the above methods do not handle prescribed landmark constraints.

2.3. Feature point mapping. Landmark-based registration has also been widely studied and different algorithms have been proposed. Bookstein et al. [2] proposed to use the thin-plate spline regularization (or biharmonic regularization) to obtain a registration that matches landmarks as much as possible. Tosun et al. [33] proposed to combine the iterative closest point registration, the parametric relaxation and the inverse stereographic projection to align cortical sulci across brain surfaces. These diffeomorphisms obtained can better match landmark features, although not perfectly. Wang et al. [26, 25, 23] proposed to compute the optimized harmonic registrations of brain cortical surfaces. The main idea is to minimize a compounded energy involving a landmark-mismatching term [22]. The obtained registration is an optimized harmonic map that better aligns landmarks. However, landmarks are not exactly matched and bijectivity cannot be guaranteed under large number of landmark constraints. To secure the bijectivity of the mapping, Joshi et al. [16] proposed the large deformation diffeomorphic metric mapping (LDDMM) to register images with a large deformation. The registration mapping can be shown to lie in the space of diffeomorphisms. Following this work, Glaunés et al. [9, 8, 34] proposed to generate large deformation diffeomorphisms with given displacements of a finite set of template landmarks. The time dependent vector fields are useful for the computation of registration with large deformations, although the computational cost of the algorithm is more expensive.

Quasi-conformal mapping that matches landmarks consistently has also been proposed [20, 24, 29, 17]. Wei et al. [37] proposed to compute landmark-matching quasi-conformal mappings for human face registration. The Beltrami coefficient associated to a landmark-matching parameterization is approximated. However, neither exact landmark matching nor the bijectivity of the mapping can be ensured when large deformations occur. Later, Lam et al. [18] proposed an iterative scheme, which provides an efficient way to obtain an exact landmark matching registration even with large deformations.

3. Mathematical Background. In this section, we describe some basic mathematical concepts related to our algorithms. For details, we refer the readers to [7, 19, 30].

A surface S with a conformal structure is called a *Riemann surface*. Given two Riemann surfaces M and N, a map $f : M \to N$ is *conformal* if it preserves the surface metric up to a multiplicative factor called the *conformal factor*. An immediate consequence is that every conformal map preserves angles. With the angle-preserving property, a conformal map effectively preserves the local geometry of the surface structure.

A generalization of conformal maps is the *quasi-conformal* maps, which are orientation preserving homeomorphisms between Riemann surfaces with bounded conformality distortion, in the sense that their first order approximations takes infinitesimal circles to infinitesimal ellipses of bounded eccentricity [7]. Mathematically, $f\colon \mathbb{C} \to \mathbb{C}$ is quasi-conformal provided that it satisfies the Beltrami equation:

$$\frac{\partial f}{\partial \overline{z}} = \mu(z)\frac{\partial f}{\partial z}. \tag{3.1}$$

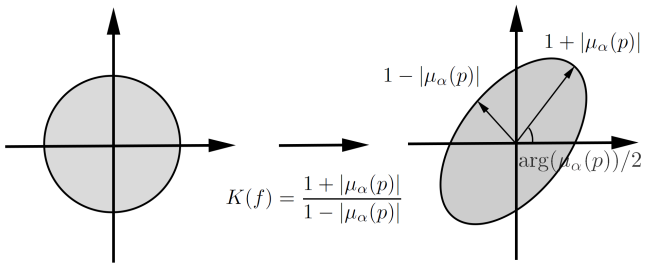

Fig. 3.1: Illustration of the relationship between a quasi-conformal map and its Beltrami differential.

for some complex-valued function μ satisfying $||\mu||_\infty < 1$. μ is called the *Beltrami coefficient*, which is a measure of non-conformality. It measures how far the map at each point is deviated from a conformal map. In particular, the map f is conformal at p when $\mu(p) = 0$. In other words, f is angle-preserving at p when $\mu(p) = 0$. Infinitesimally, around a point p, f may be expressed with respect to its local parameter as follows:

$$\begin{aligned} f(z) &\approx f(p) + f_z(p)z + f_{\overline{z}}(p)\overline{z} \\ &= f(p) + f_z(p)(z + \mu(p)\overline{z}). \end{aligned} \tag{3.2}$$

Obviously, f is not conformal if and only if $\mu(p) \neq 0$. Inside the local parameter domain, f may be considered as a map composed of a translation to $f(p)$ together with a stretch map $S(z) = z + \mu(p)\overline{z}$, which is post-composed by a multiplication of $f_z(p)$, which is conformal. All the conformal distortion of $S(z)$ is caused by $\mu(p)$. $S(z)$ is the map that causes f to map a small circle to a small ellipse. From $\mu(p)$, we can determine the angles of the directions of maximal magnification and shrinking and the amount of them as well. Specifically, the angle of maximal magnification under the stretch map is $\arg(\mu(p))/2$ with magnifying factor $1 + |\mu(p)|$; The angle of maximal shrinking under the stretch map is the orthogonal angle $(\arg(\mu(p)) - \pi)/2$ with shrinking factor $1 - |\mu(p)|$. Thus, the Beltrami coefficient μ gives us all the information about the properties of the map (See Figure 3.1).

The maximal dilation of f is given by:

$$K(f) = \frac{1 + ||\mu||_\infty}{1 - ||\mu||_\infty}. \tag{3.3}$$

4. Proposed model. In this section, we describe our proposed variational model for the optimized conformal parameterization with controllable area distortion in details.

Problem setting. Let S be a simply-connected open surface. Suppose $D \subset \mathbb{R}^2$ is our target parameter domain, which can either be a 2D rectangle or a unit disk $\mathbb{D}$. Our goal is to look for an optimized parameterization $\varphi : S \to D$, which satisfies the prescribed area distribution and minimizes the conformality distortion as good as possible. Mathematically, our problem can be formulated as follows:

$$\begin{aligned} \underset{\varphi}{\text{minimize}} \quad & E(\varphi) \\ \text{subject to} \quad & J(\varphi)\big|_{\Omega_i} = \lambda_i,\ i = 1, \ldots, m \end{aligned} \tag{4.1}$$

where $J(\varphi)$ is the Jacobian determinant of φ and $E(\varphi)$ is an energy functional that controls the conformality distortion of the parameterization φ. Note that both λ_i and Ω_i are user-defined. In addition, we assume the area distribution λ_i is prescribed according to the following condition:

$$\int_D dA - \sum_{i=1}^{m} \int_{\Omega_i} \lambda_i dA \begin{cases} = & 0 \quad \text{if} \quad \sum_{i=1}^{m} \Omega_i \equiv D \\ > & 0 \quad \text{if} \quad \sum_{i=1}^{m} \Omega_i \subset D \end{cases}$$

The above condition ensures the area distribution is correctly prescribed. More specifically, the prescribed total area of the sub-domains Ω_i's must be smaller than the total area of D.

In some situations, one might want to parameterize S in such a way that feature landmarks on S are aligned to prescribed locations in D. This type of parameterization is called the *landmark-aligned* parameterization. For example, in computer graphics, landmark aligned parameterization is required for an accurate texture mapping. For this purpose, the abovementioned model can be extended to compute a landmark-aligned optimized conformal parameterization with controllable area distortion. Denote the corresponding landmark constraints by $\{p_i \in S\}_{i=1}^{n} \leftrightarrow \{q_i \in D\}_{i=1}^{n}$. We require that $\varphi(p_i) = q_i$ for $1 \le i \le n$. The extended model can be formulated as follows.

$$\begin{aligned} \underset{\varphi: D \to S}{\text{minimize}} \quad & E(\varphi) \\ \text{subject to} \quad & \varphi(p_i) = q_i,\ i = 1, \ldots, n \\ & J(\varphi)\big|_{\Omega_i} = \lambda_i,\ i = 1, \ldots, m \end{aligned} \tag{4.2}$$

Energy model. In this subsection, we describe how we can set the energy functional E to control the conformality distortion of the parameterization.

The conformality of the parameterization φ can be measured by its Beltrami coefficient $\mu(\varphi)$. The mapping is conformal at a point p if and only if $\mu(\varphi)(p) = 0$. Hence, we define the energy functional E as follows.

$$E(\varphi) = \int_D |\mu(\varphi)|^2 + \int_D |\nabla \mu(\varphi)|^2 \tag{4.3}$$

The first energy term aims to minimize the conformality distortion. The second energy term is a regularization term that enhances the smoothness of φ.

To simplify the problem, we eliminate the hard constraint $J(\varphi)\big|_{\Omega_i} = \lambda_i$ by incorporating it into the energy functional:

$$\widetilde{E}(\varphi) = \int_D |\mu(\varphi)|^2 + \int_D |\nabla \mu(\varphi)|^2 + \alpha \left(\sum_{i=1}^{m} \int_{\Omega_i} |\log J(\varphi) - \log \lambda_i|^2 \right) \tag{4.4}$$

Here, α is called the penalty parameter. It controls how well the parameterization φ follows the prescribed area distribution. If α is set to be large, φ follows the prescribed area distortion more in the cost of losing the conformality. When α is small, the first

two energy terms are more dominant. Thus, more conformality and smoothness can be achieved, however, φ follows the prescribed area distribution less.

Furthermore, φ is required to be diffeomorphic. The bijectivity of φ can be controlled by $\mu(\varphi)$. In fact, $||\mu(\varphi)||_\infty < 1$ if and only if φ is diffeomorphic. To see this, note that the Jacobian $J(\varphi)$ of φ and $\mu(\varphi)$ are related as follows:

$$J(\varphi) = |\frac{\partial \varphi}{\partial z}|^2(1 - |\mu(\varphi)|^2). \tag{4.5}$$

Suppose $||\mu(\varphi)||_\infty < 1$, $J(\varphi) > 0$ everywhere. Hence, by the inverse function theory, φ is locally diffeomorphic. Since S is simply-connected and φ is proper, we can conclude that φ is a diffeomorphism. In fact, φ is a universal covering map of degree 1. Hence, φ must be bijective.

Our optimization problem can now be formulated as follows.

$$\begin{aligned} \underset{\varphi: D\to S}{\text{minimize}} \quad & \widetilde{E}(\varphi) := \int_D |\mu(\varphi)|^2 + \int_D |\nabla \mu(\varphi)|^2 + \alpha \left(\sum_{i=1}^m \int_{\Omega_i} |\log J(\varphi) - \log \lambda_i|^2 \right) \\ \text{subject to} \quad & (1)\ \varphi(p_i) = q_i,\ i = 1, \dots, n \\ & (2)\ \|\mu(\varphi)\|_\infty < 1 \end{aligned} \tag{4.6}$$

The above variational model (4.6) enforces hard landmark constraints. Sometimes, it may be more suitable to enforce soft landmark constraints, which allows certain degree of landmark mismatching. This situation occurs when landmarks cannot be precisely located. In the situation when exact landmark matching is not necessary, enforcing soft landmark constraints allow more conformality to be achieved. Model (4.6) can be easily modified to a variational model with soft landmark constraints by minimizing:

$$\widetilde{E}_{soft}(\varphi) = \int_D |\mu(\varphi)|^2 + \int_D |\nabla \mu(\varphi)|^2 + \alpha \int_D |\log J(\varphi) - \log \lambda|^2 + \beta \sum_{i=1}^n |\varphi(p_i) - q_i|^2. \tag{4.7}$$

subject to the constraint that $\|\mu(\varphi)\|_\infty < 1$.

Note that minimizing the above variational models (4.6) or (4.7) over φ is challenging. In particular, $\mu(\varphi)$ is defined as the quotient of first derivatives of φ, whereas $\nabla\mu(\varphi)$ involves the second derivatives of φ. The Euler-Lagrange equations of the energy functionals are complicated. To alleviate this issue, we simplify our optimization process using the splitting method. Note that the original model (4.6) is equivalent to minimizing

$$\widetilde{E}'(\nu, \varphi) = \int_D |\nu|^2 + \int_D |\nabla \nu|^2 + \alpha \left(\sum_{i=1}^m \int_{\Omega_i} |\log J(\varphi) - \log \lambda_i|^2 \right) \tag{4.8}$$

subject to (1) $\varphi(p_i) = q_i$ for $i = 1, 2, ..., n$; (2) $||\nu||_\infty < 1$ and (3) $\nu = \mu(\varphi)$.

We consider the following simplified model of the original variational problem

(4.6):

$$\begin{aligned}\underset{\nu:D\to\mathbb{C},\varphi:D\to S}{\text{minimize}} \quad & \widetilde{E}^{split}(\nu,\varphi) := \int_D |\nu|^2 + \int_D |\nabla\nu|^2 + \alpha\left(\sum_{i=1}^{m}\int_{\Omega_i} |\log J(\varphi) - \log\lambda_i|^2\right) \\ & \qquad + \gamma\int_D |\nu - \mu(\varphi)|^2 \\ \text{subject to} \quad & (1)\ \varphi(p_i) = q_i,\ i = 1,\dots,n \\ & (2)\ \|\nu\|_\infty < 1\end{aligned} \tag{4.9}$$

The last term aims to enforce the constraint (3) of the original problem (4.8) as much as possible. γ is the penalty parameter. When γ is large enough, the constraint (3) can be well satisfied. We minimize the simplified model (4.9) alternatively. That is, we minimize the model with respect to ν and φ alternatively. This will be explained in more details in the next subsection.

Similarly, the soft landmark constraint model (4.7) can also be simplified as follows by minimizing:

$$\begin{aligned}\widetilde{E}^{split}_{soft}(\nu,\varphi) = & \int_D |\nu|^2 + \int_D |\nabla\nu|^2 + \alpha\left(\sum_{i=1}^{m}\int_{\Omega_i} |\log J(\varphi) - \log\lambda_i|^2\right) + \beta\sum_{i=1}^{n}|\varphi(p_i) - q_i|^2 \\ & + \gamma\int_D |\nu - \mu(\varphi)|^2\end{aligned} \tag{4.10}$$

subject to the constraint that $\|\nu\|_\infty < 1$.

Minimization of the energy model. In this subsection, we describe how we minimize the energy models (4.9).

To simplify the problem, the surface S is firstly parameterized onto D using a conformal map $\phi : D \to S$. As a result, our problem is reduced to a 2D problem to look for an optimal map $f : D \to D$ such that the composition map $f \circ \phi^{-1}$ is our desired parameterization.

We first consider the minimization problem (4.9). With the parameterization as introduced above, our optimization problem can be formulated as:

$$\begin{aligned}\underset{\nu:D\to\mathbb{C},f:D\to D}{\text{minimize}} \quad & \widetilde{E}^{split}(\nu,f) := \int_D |\nu|^2 + \int_D |\nabla\nu|^2 + \alpha\left(\sum_{i=1}^{m}\int_{\Omega_i} |\log J(f) - \log\lambda_i|^2\right) \\ & \qquad + \gamma\int_D |\nu - \mu(f)|^2 \\ \text{subject to} \quad & (1)\ f\circ\phi^{-1}(p_i) = q_i,\ i = 1,\dots,n \\ & (2)\ \|\nu\|_\infty < 1\end{aligned} \tag{4.11}$$

Conventional penalty method increases the penalty parameter γ in each iteration until ∞. To further improve the efficiency of the algorithm, we fix the penalty parameter γ to be a large enough constant and solve only one optimization problem.

Suppose we are in the n^{th} iteration with (ν_n, f_n), we first consider the derivative of the area mismatching term $E_{area}(f) = \int_\Omega |\log J(f) - \log\lambda|^2$. Here, we simplify our discussion by considering Ω only.

Now we wish to find the function v adding to f_n so that the area mismatching term $E(f+\epsilon v)$ decreases, for some small value of ϵ. More precisely, we wish to find the first variational of $E(f_n)$ such that $E(f_n+\epsilon v)$ decreases most rapidly. The desired direction is simply the negative of the functional derivative. Consider

$$\begin{aligned}
&\frac{d}{d\epsilon}E_{area}(f_n+\epsilon v)\Big|_{\epsilon=0}\\
=&\int_\Omega \frac{\partial}{\partial\epsilon}\left(|\log J(f_n+\epsilon v)-\log\lambda|^2\right)\Big|_{\epsilon=0}\\
=&\int_\Omega \frac{2}{J(f_n+\epsilon v)}\left(\log J(f_n+\epsilon v)-\log\lambda\right)\frac{d}{d\epsilon}J(f_n+\epsilon v)\Big|_{\epsilon=0}\\
=&\int_\Omega \frac{4}{J(f_n)}(\log J(f_n)-\log\lambda)\left(\frac{\partial f_n^1}{\partial x}\frac{\partial v_2}{\partial y}+\frac{\partial f_n^2}{\partial y}\frac{\partial v_1}{\partial x}-\frac{\partial f_n^1}{\partial y}\frac{\partial v_2}{\partial x}-\frac{\partial f_n^2}{\partial x}\frac{\partial v_1}{\partial y}\right)
\end{aligned}$$

where $f_n=(f_n^1,f_n^2):\mathbb{R}^2\to\mathbb{R}^2$ and $v=(v_1,v_2):\mathbb{R}^2\to\mathbb{R}^2$. By using integration by parts, we have

$$\begin{aligned}
&<\nabla E_{area}(f_n),v>\\
=&\frac{d}{d\epsilon}E_{area}(f_n+\epsilon v)\Big|_{\epsilon=0}
\end{aligned}$$

$$\begin{aligned}
=&\int_\Omega\left[\frac{\partial}{\partial x}\left(\frac{4}{J(f_n)}(\log J(f_n)-\log\lambda)\frac{\partial f_n^2}{\partial y}\right)-\frac{\partial}{\partial y}\left(\frac{4}{J(f_n)}(\log J(f_n)-\log\lambda)\frac{\partial f_n^2}{\partial x}\right)\right]v_1\\
&+\left[\frac{\partial}{\partial y}\left(\frac{4}{J(f_n)}(\log J(f_n)-\log\lambda)\frac{\partial f_n^1}{\partial x}\right)-\frac{\partial}{\partial x}\left(\frac{4}{J(f_n)}(\log J(f_n)-\log\lambda)\frac{\partial f_n^1}{\partial y}\right)\right]v_2
\end{aligned}$$

Therefore, the functional derivative ∇E is obtained. By taking the negative of ∇E, we have the descent direction:

$$df_n=-\begin{pmatrix}\frac{\partial}{\partial x}\left(\frac{4}{J(f_n)}(\log J(f_n)-\log\lambda)\frac{\partial f_n^2}{\partial y}\right)-\frac{\partial}{\partial y}\left(\frac{4}{J(f_n)}(\log J(f_n)-\log\lambda)\frac{\partial f_n^2}{\partial x}\right)\\ \frac{\partial}{\partial y}\left(\frac{4}{J(f_n)}(\log J(f_n)-\log\lambda)\frac{\partial f_n^1}{\partial x}\right)-\frac{\partial}{\partial x}\left(\frac{4}{J(f_n)}(\log J(f_n)-\log\lambda)\frac{\partial f_n^1}{\partial y}\right)\end{pmatrix} \tag{4.12}$$

Once we have found df_n, the mapping is updated to be $f_n+\kappa df_n$ for some step-size κ. Determining a suitable step-size is important for the minimization process, which will be discussed in Section 5.3.

From the new mapping $f_n+\kappa df_n$ and the Beltrami equation, we know that the Beltrami coefficient is also perturbed by some μ_{df_n}. Note that

$$\frac{\partial f_n+\kappa df_n}{\partial\bar{z}}=(\mu(f_n)+\mu_{df_n})\frac{\partial f_n+\kappa df_n}{\partial z} \tag{4.13}$$

By a simple calculation, we obtain

$$\mu_{df_n}=\kappa\left(\frac{\partial df_n}{\partial\bar{z}}-\mu(f_n)\frac{\partial df_n}{\partial z}\right)\Big/\frac{\partial f_n+\kappa df_n}{\partial z} \tag{4.14}$$

From above, we transform the displacement df_n of the mapping f_n to the variation of the Beltrami coefficient μ_{df_n}. Similarly, we can compute the decent direction for the energy term $\int_D |\nu_n - \mu(f_n)|^2$, which is given by:

$$d\mu_p = 2(\nu_n - \mu(f_n)) \tag{4.15}$$

Therefore, the decent direction for the energy term

$$\alpha \left(\sum_{i=1}^{m} \int_{\Omega_i} |\log J(f_n) - \log \lambda_i|^2 \right) + \gamma \int_D |\nu_n - \mu(f_n)|^2$$

is given by $d\mu = \mu_{df_n} + \gamma d\mu_p$. We then update μ_n to $\tilde{\mu} = \mu_n + t d\mu$ for some small step-size t.

To sum up, the above discussion tells us how to update the Beltrami coefficient so as to minimize:

$$\alpha \left(\sum_{i=1}^{m} \int_{\Omega_i} |\log J(f_n) - \log \lambda_i|^2 \right) + \gamma \int_D |\nu_n - \mu(f_n)|^2 \tag{4.16}$$

We can then solve the Beltrami equation with $\tilde{\mu}$ as the Beltrami coefficient, while enforcing the landmark constraints $f \circ \phi^{-1}(p_i) = q_i$, $i = 1, 2, \ldots, n$. We then obtain the corresponding mapping $\tilde{f}$, whose Beltrami coefficient closely resembles to $\tilde{\mu}$. Note that this mapping satisfies the hard landmark constraints. Since $\tilde{\mu}$ may not be admissible with the landmark constraints enforced, the Beltrami coefficient of $\tilde{f}$ may not be exactly equal to $\tilde{\mu}$. We set $\mu_{n+1} = \mu(\tilde{f})$.

In this paper, we solve the Beltrami equation using the *Linear Beltrami Solver (LBS)* as introduced in [21]. We will now describe LBS briefly. In fact, the Beltrami equation can be reduced to two elliptic PDEs. We write $f = u + \sqrt{-1}v$. From the Beltrami equation (3.1),

$$\mu = \frac{(u_x - v_y) + \sqrt{-1}\ (v_x + u_y)}{(u_x + v_y) + \sqrt{-1}(v_x - u_y)} \tag{4.17}$$

Suppose $\mu = \rho + \sqrt{-1}\ \tau$. Then:

$$\nabla \cdot \left(A \begin{pmatrix} u_x \\ u_y \end{pmatrix} \right) = 0 \ \text{ and } \ \nabla \cdot \left(A \begin{pmatrix} v_x \\ v_y \end{pmatrix} \right) = 0 \tag{4.18}$$

Here, $A = \begin{pmatrix} \alpha_1 & \alpha_2 \\ \alpha_2 & \alpha_3 \end{pmatrix}$ is symmetric positive definitie where $\alpha_1 = \frac{(\rho-1)^2+\tau^2}{1-\rho^2-\tau^2}$; $\alpha_2 = -\frac{2\tau}{1-\rho^2-\tau^2}$ and $\alpha_3 = \frac{1+2\rho+\rho^2+\tau^2}{1-\rho^2-\tau^2}$.

Hence, given μ, the quasi-conformal map f can be reconstructed by solving (4.18) subject to the landmark constraints. In the discrete case, the elliptic PDEs (4.18) can be discretized as two linear systems subject to the landmark constraints. Such a solver for quasi-conformal map is called the *Linear Beltrami Solver (LBS)*. For details, please refer to [21].

With the new Beltrami coefficient μ_{n+1}, our next step is to minimize the energy terms

$$\int_D |\nu|^2 + \int_D |\nabla \nu|^2 + \gamma \int_D |\nu - \mu_{n+1}|^2 \tag{4.19}$$

with respect to ν. Note that these terms act as the regularizer of the energy model as well as minimizing the Beltrami coefficient to enforce the bijectivity constraint. By considering the Euler-Lagrange equation, the optimization problem (4.19) is equivalent to solving

$$(-\Delta + 2I + 2\gamma I)\,\nu = 2\gamma\mu_{n+1} \tag{4.20}$$

Once we have solved for ν_{n+1} satisfying the Euler-Lagrange equation (4.20), we can update f_{n+1} by solving the Beltrami equation with $\mu = \nu_{n+1}$ using LBS. We repeat the above process until $\|\mu(f_{n+1}) - \mu(f_n)\|_\infty \leq \epsilon$ for some small threshold ϵ.

The overall algorithm can now be summarized as follows:

Algorithm 1: *Optimized conformal parameterization with controllable area distortion*

Input: Surface S and its conformal parameterization ϕ; Prescribed area distribution λ; Boundary condition for the target domain D.

Output: Optimized parameterization $f \circ \phi^{-1} : S \to D$ balancing between the area distortion and conformality distortion.

Initial $\nu_0 = 0$; $f_0 = Id$; $\mu_0 = 0$;
repeat
  Compute df minimizing the area mismatching term;
  Compute the step-size κ as described in Section 5.3;
  Compute $\tilde{\mu} = \mu(f + \kappa df)$;
  Use LBS to reconstruct $\tilde{f}$ from $\tilde{\mu}$ with landmark constraints;
  Compute $\mu_{n+1} = \mu(\tilde{f})$;
  Solve ν_{n+1} from the Euler-Lagrange equation

$$(-\Delta + 2I + 2\gamma I)\,\nu = 2\gamma\mu_{n+1};$$

  Use LBS to reconstruct f_{n+1} from ν_{n+1} with landmark constraints;
  Compute $\mu(f_{n+1})$;
until $||\mu(f_{n+1}) - \mu(f_n)||_\infty \leq \epsilon$;

5. Numerical implementation. In this section, we discuss the numerical implementation of our proposed algorithm in details.

5.1. Discrete differential operators. Consider a triangle $T = [v_1, v_2, v_3]$ where $v_k = x_k + iy_k$ for $k = 1, 2, 3$. Suppose we have a function f on the triangle. By the first order approximation

$$f(z) \approx f(p) + f_z(p)z + f_{\bar{z}}\bar{z} \tag{5.1}$$

we have the following equality on each triangle in the triangulation mesh:

$$\begin{pmatrix} f(v_1) \\ f(v_2) \\ f(v_3) \end{pmatrix} = \begin{pmatrix} v_1 & \overline{v_1} & 1 \\ v_2 & \overline{v_2} & 1 \\ v_3 & \overline{v_3} & 1 \end{pmatrix} \begin{pmatrix} f_z(p) \\ f_{\bar{z}}(p) \\ f(p) \end{pmatrix} \tag{5.2}$$

where p is any interior point in the triangle. By solving this equation on each triangle, we can define the discrete differential operator D_z and $D_{\bar{z}}$ explicitly. With the discrete

differential operator D_z and $D_{\bar{z}}$, we can obtain the discrete Beltrami coefficients directly.

Let $T_1 = [v_i, v_j, v_k]$ and $T_2 = [v_i, v_j, v_l]$. The mesh Laplacian is defined as:

$$\Delta(f(v_i)) = \sum_{T \in N_i} \frac{\cot \alpha_{ij} + \cot \beta_{ij}}{2} (f(v_j) - f(v_i)) \tag{5.3}$$

where α_{ij} and β_{ij} are the two interior angles of T_1 and T_2 which are opposite to the edge $[v_i, v_j]$ [13].

5.2. Descent direction for the area mismatching term. Recall that the descent direction of the area mismatching term in equation (4.12):

$$df_n = -\begin{pmatrix} \frac{\partial}{\partial x}\left(\frac{4}{J(f_n)}(\log J(f_n) - \log\lambda)\frac{\partial f_n^2}{\partial y}\right) - \frac{\partial}{\partial y}\left(\frac{4}{J(f_n)}(\log J(f_n) - \log\lambda)\frac{\partial f_n^2}{\partial x}\right) \\ \frac{\partial}{\partial y}\left(\frac{4}{J(f_n)}(\log J(f_n) - \log\lambda)\frac{\partial f_n^1}{\partial x}\right) - \frac{\partial}{\partial x}\left(\frac{4}{J(f_n)}(\log J(f_n) - \log\lambda)\frac{\partial f_n^1}{\partial y}\right) \end{pmatrix}$$

or in the complex form:

$$df_n = -\left(\frac{\partial}{\partial \bar{z}}\right)\left(\frac{8}{J(f_n)}(\log J(f_n) - \log\lambda)\frac{\partial f_n}{\partial z}\right) + \left(\frac{\partial}{\partial z}\right)\left(\frac{8}{J(f_n)}(\log J(f_n) - \log\lambda)\frac{\partial f_n}{\partial \bar{z}}\right)$$

where $f_n = f_n^1 + i f_n^2$. By the discretization of the differential operator introduced in section 5.1, we have the discrete version of the descent direction;

$$df_n = -D_z^* (M D_z f_n) + D_{\bar{z}}^* (M D_{\bar{z}} f_n) \tag{5.4}$$

where M is a diagonal matrix with elements $\frac{8}{J(f_n)} (\log J(f_n) - \log\lambda)$ defined on each triangle of the mesh and D^* is the conjugate transpose of a matrix D.

5.3. Choice of the parameter. After the decent direction df reducing the area mismatching energy term is found, we also need to choose the step-size κ. κ is chosen as follows:

Algorithm 2: *Step-size* κ

Input: Triangular mesh with vertex v; Descent direction df.

1 Initial $\kappa = 1$;

2 Find κ such that

$$\kappa^* = \max_{0<\kappa\leq 1} \left\{\kappa \| \det(v + \kappa df) > 0 \ for \ \forall \text{ triangle } v = [v_1, v_2, v_3]^T\right\};$$

3 If $\kappa^* < 1$, update $\kappa \leftarrow \kappa^*$;

To solve for κ^*, let $v_i = [x_i, y_i]$ and $df(v_i) = [dx_i, dy_i]$ respectively. We further denote $x_{ij} = x_i - x_j$ for simplicity. Then consider the following

$$\det\left[\begin{pmatrix} x_1 & x_2 & x_3 \\ y_1 & y_2 & y_3 \\ 1 & 1 & 1 \end{pmatrix} + \kappa \begin{pmatrix} dx_1 & dx_2 & dx_3 \\ dy_1 & dy_2 & dy_3 \\ 0 & 0 & 0 \end{pmatrix}\right] = A\kappa^2 + B\kappa + C$$

where

$$A = dx_{21}dy_{31} - dx_{31}dy_{21}$$
$$B = dx_{21}y_{31} + dy_{31}x_{21} - dx_{31}y_{21} - dy_{21}x_{31}$$
$$C = x_{21}y_{31} - x_{31}y_{21}$$

Therefore, by considering the above quadratic equation, we can determine the condition on κ that guarantees the preservation of the orientation for each triangle, i.e. avoiding flips of triangles on the mesh.

6. Experimental results. We have tested our proposed algorithm on both synthetic and real data. In this section, we report the experimental results.

6.1. Synthetic examples.

Example 1. We first test our proposed model on a synthetic example, whose area distribution is prescribed as an expanding ball in the center of the rectangular mesh. In this example, the regularization terms in our model

$$\int_D |\nu|^2 + |\nabla\nu|^2$$

are removed. The aim is to check whether the area mismatching term can effectively enforce the prescribed area distribution. Figure 6.1(a) shows the original domain S to be parameterized, which is just a 2D rectangular mesh. S is deformed, under which the central disk is enlarged, which is shown in (b). (c) shows the logarithm of the Jacobian determinant of the deformation, visualized by a colormap. It is used to define the area distribution in this example. Figure 6.2(a) shows the result obtained by our algorithm. Although the area distribution can be matched accurately, conformality distortion is large, especially on the region near the boundary of the ball. Figure 6.2(b) shows the energy versus iterations in the algorithm. Since regularization terms are not considered, a zero energy means an exact matching of the area distribution. (c) shows the distribution of the conformality distortion. Note that the regularization terms are removed and hence the conformality distortion of the parameterization is not under control. Some triangles have large Beltrami coefficients with $\mu > 0.75$, which indicate large conformality distortions.

Example 2. In the second example, we include the both regularization term (with the corresponding coefficient equal to 1) and area distortion term with coefficient $\alpha = 0.3$. As shown in Figure 6.3(a), instead of having an exact matching of area distribution, the regularization terms prevent the triangles on the boundary of the ball from being squeezed. The magnitude of the area mismatching $\log J(f) - \log\lambda$ is relatively larger when comparing with other regions. However, as shown in Figure 6.3(c), the maximal conformality distortion, which is expressed as the norm of the Beltrami coefficient μ, is smaller (with $\|\mu\|_\infty = 0.4609$). It means the obtained parameterization preserves more conformality.

Example 3. We have also tested the same setup with $\alpha = 0.1$. By decreasing the parameter α, the conformality distortion becomes less when comparing with Example 1 and Example 2 (See Figure 6.4(c)). However, the mis-matching of the prescribed area distribution is bigger than that in Example 1 and 2. In these examples, we can observe that there is always a balance between the area distortion and conformality distortion of the parameterization. The parameter α is therefore a convenient tool to control the balance.

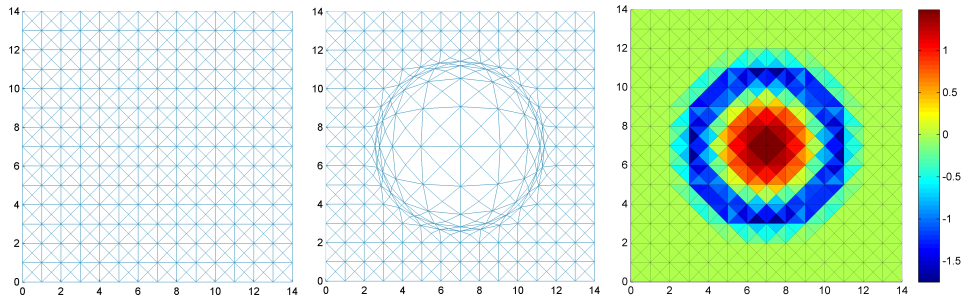

(a) (b) (c)

Fig. 6.1: Setup in Example 1. (a) shows the original mesh S, which is a 2D square domain. The original mesh S is deformed, under which the central disk is enlarged, as shown in (b). (c) shows the logarithm of the Jacobian determinant of the deformation, visualized by a colormap. It is used to define the area distribution in Example 1.

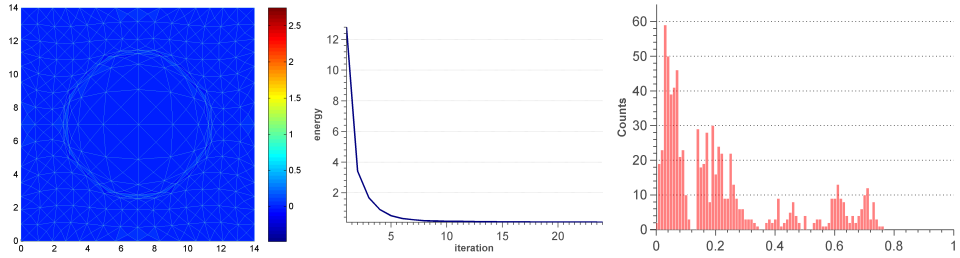

(a) (b) (c)

Fig. 6.2: Result of Example 1 without considering the regularization terms. (a) shows the optimized parameterization that matches the prescribed area distribution. (b) shows the plot of energy versus iterations in the algorithm. (c) shows the histogram of magnitude of the Beltrami coefficient, which describes the distribution of the conformality distortion under the optimized parameterization.

Example 4. In this example, we define the area distribution λ such that $\log \lambda$ is compactly supported in a small region (the red region in Figure 6.5(a)). The colormap on Figure 6.5(a) is given by $\log \lambda$. In other words, we aim to obtain a parameterization, which enlarges the area of the interesting (red) region. We set $\alpha = 10/3$ to balance between area and conformality distortions of the parameterization. (b) shows the parameterization result, whose colormap is given by $\log J$. As expected, the red region is enlarged under the parameterization. Note that $\log J$ is not exactly equal to the input $\log \lambda$, since a non-zero α is set to balance between the matching of area distribution and conformality distortion. (c) shows the plot of the energy versus iterations. Note that the energy is minimized iteratively. (d) shows the magnitude of the Beltrami coefficient asssociated to the obtained parameterization.

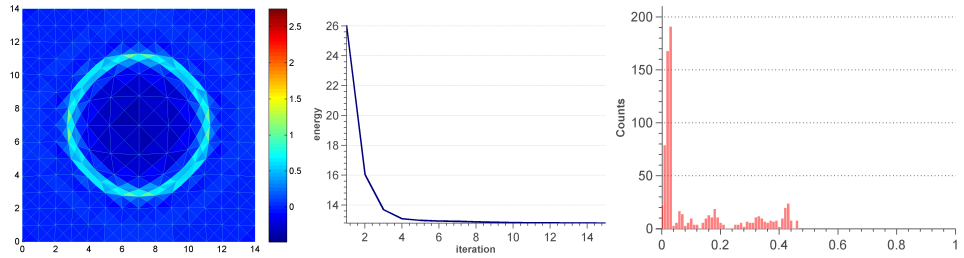

(a) (b) (c)

Fig. 6.3: Results of Example 2. (a) shows the optimized parameterization in Example 2, in which the regularization terms are included in the model with $\alpha = 0.3$. (b) shows the plot of energy versus iterations in the algorithm. (c) shows the histogram of magnitude of the Beltrami coefficient, which describes the distribution of the conformality distortion under the optimized parameterization.

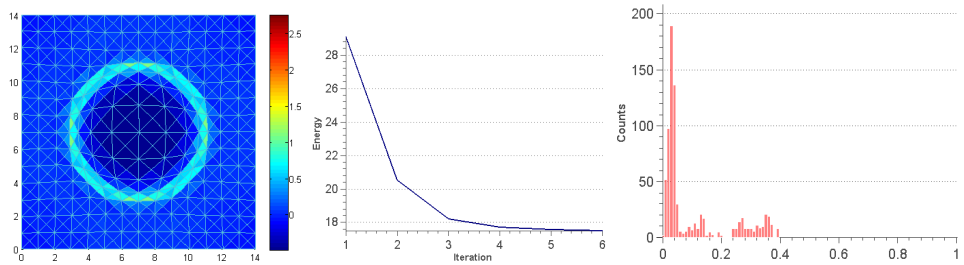

(a) (b) (c)

Fig. 6.4: Results of Example 3. (a) shows the optimized parameterization in Example 2, in which the regularization terms are included in the model with $\alpha = 0.1$. (b) shows the plot of energy versus iterations in the algorithm. (c) shows the histogram of magnitude of the Beltrami coefficient, which describes the distribution of the conformality distortion under the optimized parameterization.

Example 5. In this example, we test our algorithm to compute optimized conformal parameterization with landmark constraints enforced. Figure 6.6(a) shows the landmark points p_i on S and their target positions q_i, which are represented by blue and red dots respectively. We set $\lambda \equiv 1$ on the whole domain in this example. In other words, we aim to compute an optimized parameterization of S onto a 2D rectangle D, which satisfies the landmark constraints while preserving the area as much as possible. (b) shows the parameterization when we set $\alpha = 0$. The colormap is given by $\log J$. It can be observed that triangular faces in the middle region are squeezed drastically. It is expected since area distortion term is removed in the model. (c) shows the parameterization result when we set $\alpha = 1$. As the area distortion term is included in the model, the squeezing of triangular faces are eliminated. (d) shows the energy plot versus iteration and (e) shows the conformality distortion of the parameterization.

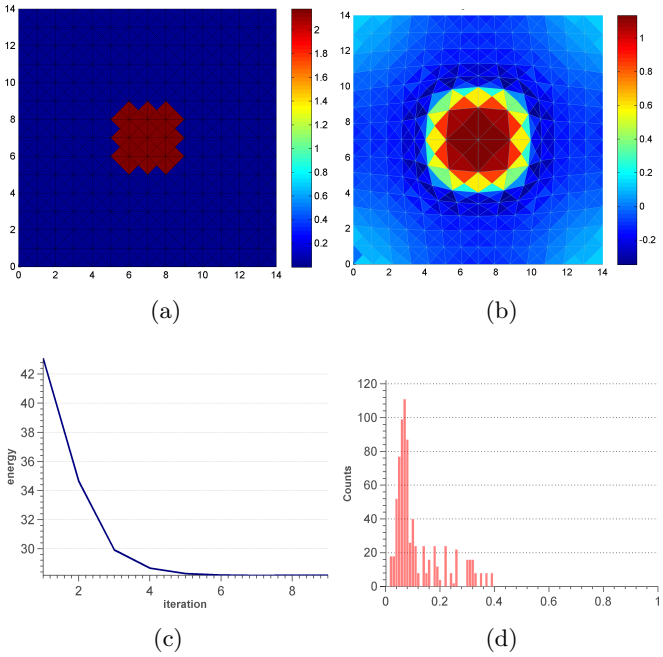

Fig. 6.5: Results of Example 4. S is again chosen as the square mesh. (a) shows the area distribution $\log \lambda$, which is compactly supported in the red region. (b) shows the optimized parameterization obtained from our algorithm. The colormap is given by the logarithmic of the Jacobian determinant of the parameterization. (c) shows the plot of energy versus iterations in the algorithm. (d) shows the histogram of the magnitude of the Beltrami coefficient.

Example 6. We have also tested our proposed algorithm on 3D surface S. One of the application of such an optimized parameterization is for texture mapping. In this example, we are given a surface mesh S and a texture image (See Figure 6.7(a)). We will parameterize S onto a rectangular domain D such that the area distribution is consistent with the area distribution of the surface S. We first conformally parameterize the 3D surface onto D. Using the conformal parameterization, we map the texture image onto S, which is shown in (b). Observe that the characters "8" and "5" are enlarged and distorted unnaturally at the bumps. (c) shows the optimized conformal parameterization minimizing the area distortion. The colormap is given by the area distribution mismatching in logarithmic scale. Note that the difference are close to zero, meaning that the area distribution of the parameterization closely resembles to that of S. (d) shows the textured surface using the obtained optimized parameterization. Note that the distortions of the characters $''8''$ and $''5''$ at the bumps are avoided. (e) and (f) shows the energy versus iterations and the conformality distortion of the optimized parameterization respectively.

6.2. Real examples. We have also tested our proposed model on real data.

Brain surface parameterization. The complicated structure of the brain hinders the shape analysis of brain cortical surfaces. To alleviate this issue, parameter-

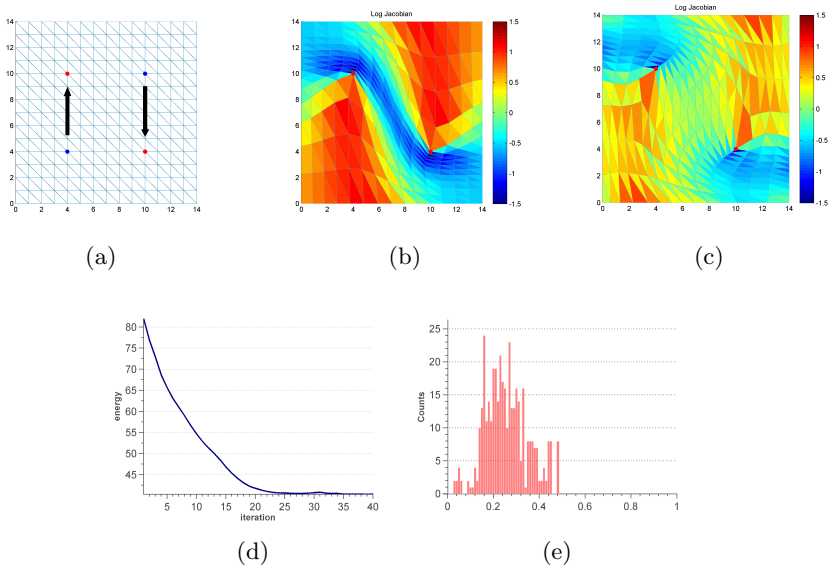

(a) (b) (c)

(d) (e)

Fig. 6.6: Results of Example 5. (a) shows the original domain S and the landmark points denoted by blue dots. Their target positions are denoted by red dots. (b) shows the landmark-aligned optimized parameterization with $\alpha = 0$. The colormap is given by the logarithmic Jacobian determinant of the parameterization. (c) shows the landmark-aligned optimized parameterization with $\alpha = 1$. The colormap is given by the logarithmic Jacobian determinant of the parameterization. (d) shows the plot of energy versus iterations and (e) shows the conformality distortion of the parameterization.

ization techniques are often used to flatten the cortical surface, so that the analysis and computation can be carried out on the 2D domain. Conformal parameterizations have been widely used since they preserve the local geometry well. Hence, local geometric structures of the brain cortical surface can be visualized on the 2D domain. However, the major drawback of a conformal parameterization is that it may introduce area distortion, such as a serious squeezing. This causes difficulties to visualize the geometric structure of the brain on the parameter domain. Using our proposed algorithm, we can obtain an optimized parameterization that balances between conformality and area distortions. Figure 6.8(a) shows a human brain cortical surface. Its conformal parameterization is shown in (b). It can be observed that a large portion of the surface are squeezed onto the central region of the parameter domain under the parameterization. (c) shows the optimized parameterization obtained from our proposed model. The squeezing effect on the parameter domain is avoided, while the geometric pattern of the sulci can be well observed.

Surface parameterization. We have also tested our proposed algorithm on real 3D surfaces. In this example, we parameterize a lion head surface with prescribed area distribution, so as to enlarge the interesting region on the parameter domain. The lion head surface is shown in Figure 6.9(a). The area distribution is defined such that the mouth and eyes of the lion head are enlarged on the parameter domain. (b) shows

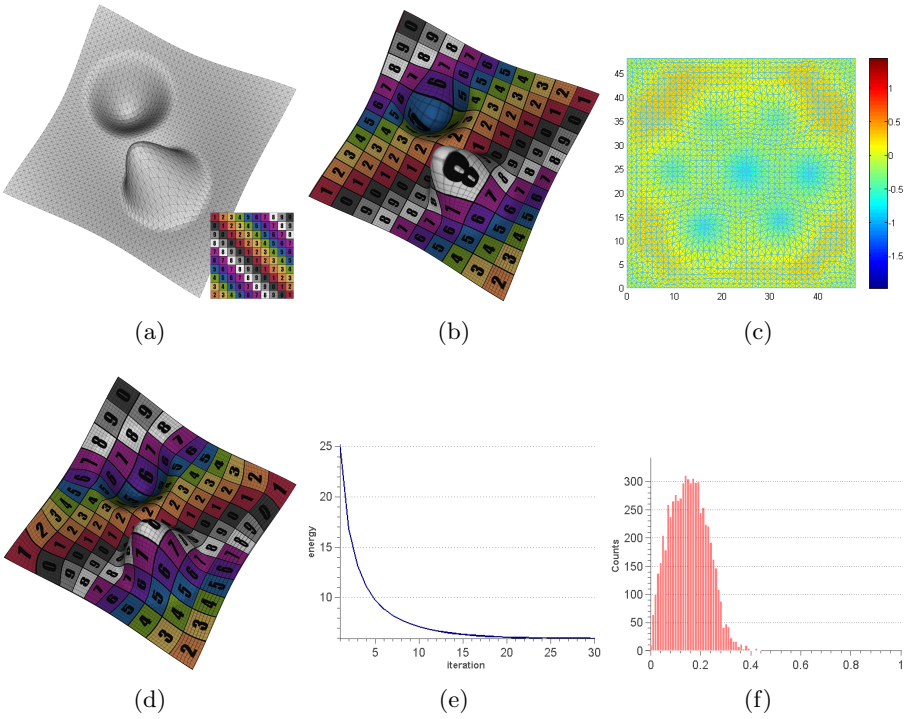

Fig. 6.7: (a) shows a surface mesh S and the texture image. (b) shows the textured surface using the conformal parameterization. (c) shows the optimized conformal parameterization that minimizes area and conformality distortions. (d) shows the textured surface using the optimized parameterization. (e) shows the plot of energy versus iterations. (f) shows the conformality distortion of the parameterization.

the conformal parameterization of the lion head surface, whose colormap is given by the prescribed area distribution $\log \lambda$. (c) shows the conformal parameterization of the lion head, whose colormap is given by the curvature of the surface. (d) shows the optimized parameterization obtained using our algorithm. Using our proposed algorithm with the prescribed area distribution, we successfully enlarge the mouth and eyes. The result is shown in Figure 6.9(d). The shapes of the mouth and eyes can be observed on the parameter domain.

Vertebral bone registration. An important application of parameterizations is to compute surface registration. Once the landmark-aligned parameterizations of two surfaces are obtained, a landmark-matching registration between the two surfaces can be easily computed through the composition map of the parameterizations. In this example, we tested our model to register genus-one surfaces with prescribed landmark constraints. Figure 6.10 (a) shows the surface mesh of a vertebrae bone A. Feature landmark points are marked as blue dots. Its conformal parameterization onto the universal covering space is shown in (b). The feature landmarks points on the parameter domain are also represented by the blue dots, which are located in the dense region of the parameterized mesh. Note that we applied the parameterization

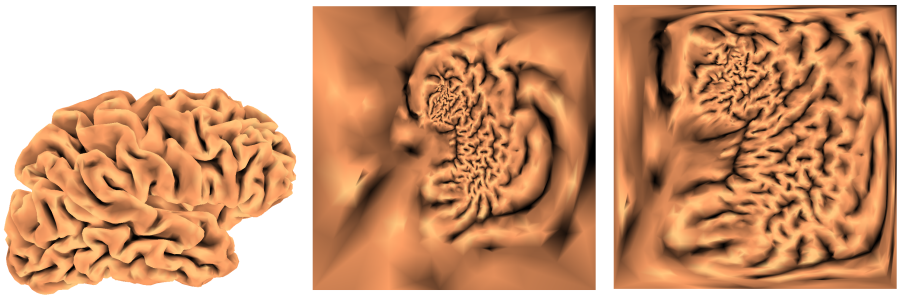

(a) (b) (c)

Fig. 6.8: (a) shows the brain cortical surface. The colormap is given by the mean curvature of the brain surface. (b) shows the conformal parameterization. (c) shows the optimized parameterization, which minimizes both the area and conformality distortions.

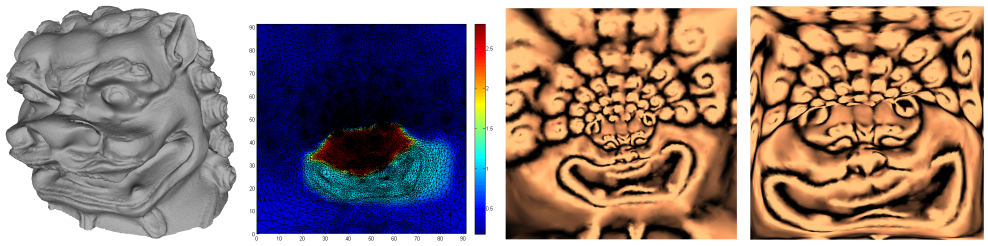

(a) (b) (c) (d)

Fig. 6.9: (a) shows the surface mesh of a lion head. (b) shows the prescribed area distribution $\log \lambda$, shown on the conformal parameter domain. (c) shows the comformal parameterization. (d) shows the optimized parameterization obtained from our proposed model.

algorithm proposed in [14] and a periodic boundary condition must be satisfied. Figure 6.10(c) and (d) show the surface mesh of a vertebrae bone B and its conformal parameterization respectively. The red dots in (c) and (d) represent the feature landmark points of vertebrae bone B. To register bone A onto bone B, we parameterize bone A such that its landmark points are mapped to the landmark points of bone B on its parameter domain. Our goal is to obtain a landmark-aligned optimized parameterization, which balances between area and conformality distortions. (e) shows the optimized parameterization result of bone A. Using the composition map of the parameterization, we deform bone A to bone B, which is shown in (f). This gives the surface registration between the two surface meshes. (g) shows the histogram of the logarithmic Jacobian determinant of the overall mapping. The distribution is accumulated at zero, indicating that most of the triangles in the surface mesh preserve area under the mapping.

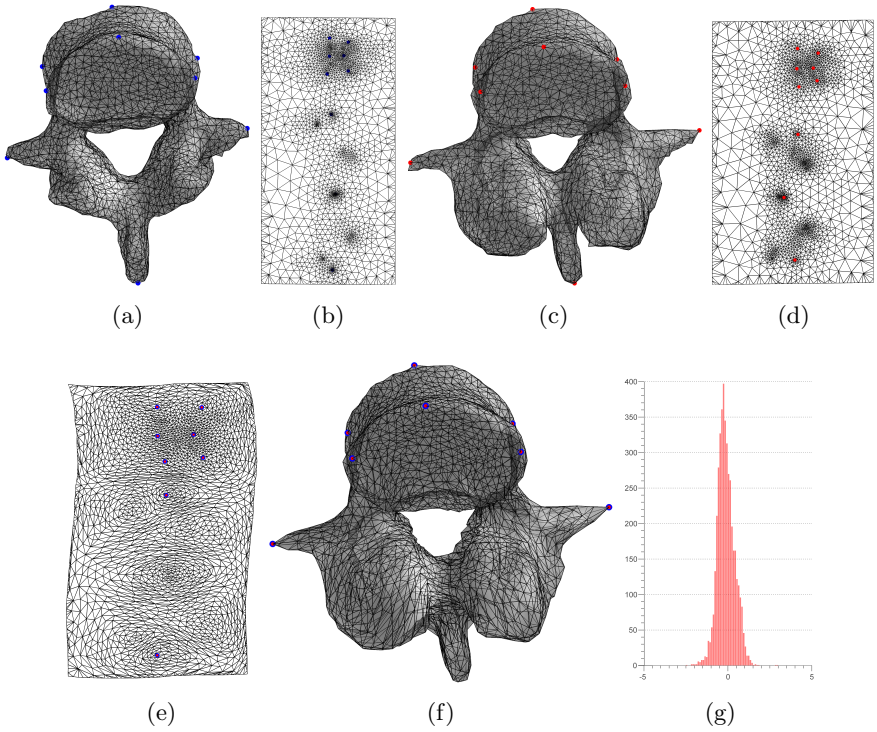

Fig. 6.10: (a) shows the surface mesh of Vertebrae bone A. Feature landmark points are marked as blue dots. (b) shows the conformal parameterization of bone A onto its universal covering space. (c) shows the surface mesh of Vertebrae bone B. Corresponding feature landmark points are marked as red dots. (d) shows the conformal paramterization of bone B onto its universal covering space. (e) shows the landmark-aligned optimized parameterization, which minimizes both the conformal and area distortions. Using the composition map of the parameterizations, we deform bone A to bone B, which is shown in (f). (g) shows the histogram of the logarithmic Jacobian determinant of the overall mapping.

Visualization of surface-based protein. In this example, we tested our algorithm to parameterize protein surfaces to facilitate the visualization of protein structures. The protein data are obtained from the RCSB Protein Data Bank(PDB). We have chosen proteins with ID 4CS4 and 4D2I in our experiment. The motivation to study the surface of a protein is that the 3 dimensional structures of proteins can give useful information to determine their functionalities, through the comparison with other well-studied proteins. In particular, the electrostatic surface of a protein is an important information to study the protein-protein interaction [31]. Figure 6.11(a) and (b) show the surface representations of proteins 4CS4 and 4D2I respectively. The red regions denote the particular regions we are interested in. (c) and (d) show the electrostatic surfaces of proteins 4CS4 and 4D2I respectively. The electrostatic properties of the protein are calculated by solving the Poisson-Boltzmann equation [5]. The zoom-in of the selected regions with electrostatic information are shown in (e)

and (f).

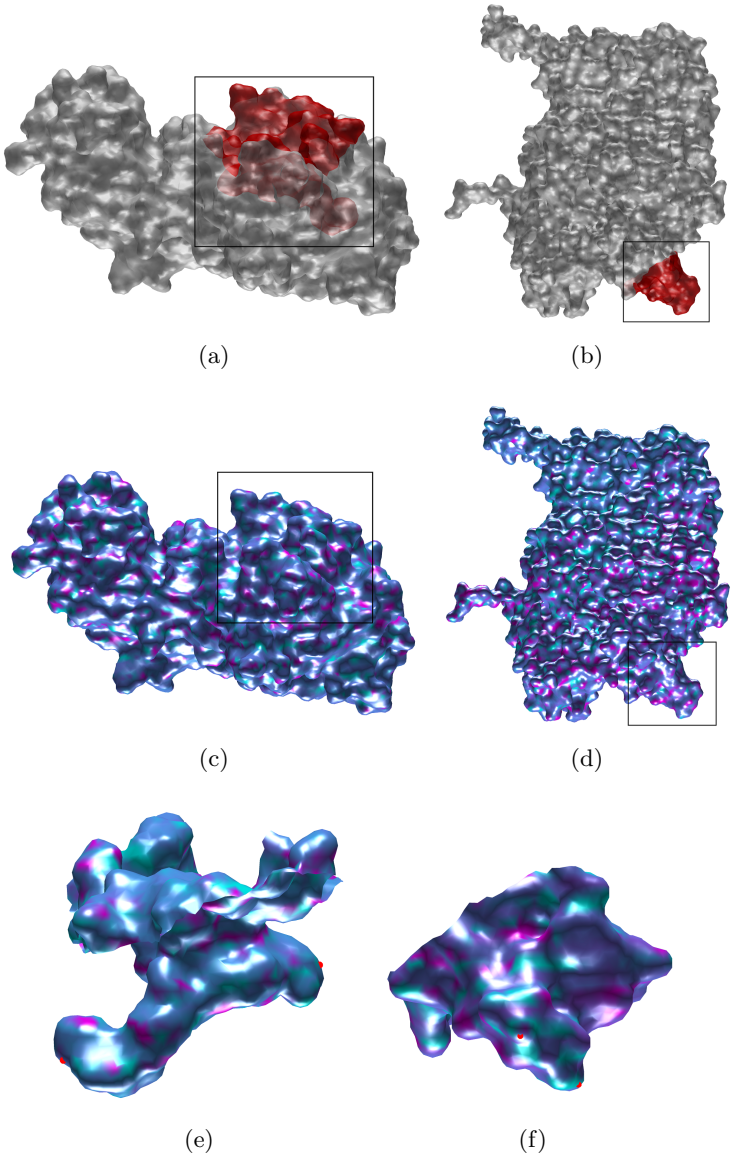

Fig. 6.11: (a) shows the surface representation of the protem with ID 4CS4. A selected region is labeled in red. (b) shows the surface representation of the protein with ID 4D2I. A selected region is labeled in red. (c) shows the electrostatic information of the proteins in (a). (d) shows the electrostatic information of the proteins in (b). (e) shows the zoom-in of the selected red region of (a). (f) shows the zoom-in of the selected red region of (b).

To test our algorithm, we parameterize the selected region of each protein with landmark constraints enforced (so that regions of interest are aligned consistently

for the ease of shape comparison). In addition, we set the area distribution of each selected region, such that the red sub-region is enlarged on the parameter domain (See Figure 6.12(a) and (b)). (c) and (d) show the conformal parameterization of the two selected regions. The purple and the blue colors indicate the positive and negative potential respectively. The distribution of the potential play a significant role on the binding between proteins, defining mechanisms of protein-protein complex formation as well as the study of protein movements [32]. Notice that the red regions are squeezed on the conformal parameter domains in both cases. This hinders the visualization and shape comparison of protein structures on the 2D parameter domain. Using our proposed algorithm, we aim to obtain protein parameterizations which balance between area and conformality distortion. Two landmarks are delineated on each protein surface. The green dots in (c) and (d) denote the locations of landmarks on the conformal parameter domain. In order to compare the two proteins, we fix the parameter domain for both surfaces as a 2D rectangle of certain dimensions. Corresponding feature landmarks are also required to be aligned consistently on the parameter domain. (e) and (f) show the parameterization results. Note that corresponding landmarks are indeed aligned consistently. Also, unlike the conformal parameterizations, the red regions of the proteins are not squeezed on the parameter domain under our parameterizations. Our algorithm can produce optimized parameterizations, which give good balances between area and conformality distortions. This allows us to visualize the electrostatic information in the interested (red) regions on the 2D parameter domain more effectively. The energies versus iterations of our algorithm to compute the parameterizations of (a) and (b) are shown in (g) and (h) respectively. Figure 6.13(a) and (b) give a clearer visualization of the parameterized meshes, whose colormaps are given by their electostatic information.

7. Conclusion. This paper presents a new approach to obtain a landmark constrained surface parameterization which balances between the conformal and area distortions. Furthermore, the area distribution of the surface parameterization can be prescribed by users to fit their applications. The main strategy is to minimize an energy functional involving the area mismatching term and the regularization term involving the Beltrami coefficient. The Beltrami coefficient measures the conformality distortion of the quasiconformal map. It also helps controlling the bijectivity and smoothness of the parameterization. Experiments have been carried out on both synthetic and real data. Results show that our proposed method can effectively control the area distribution as well as the conformality distortion of the parameterization. In the future, we plan to extend our proposed algorithm to 3D volumetric data and apply our proposed algorithm to medical imaging for diseases analysis.

REFERENCES

[1] Haker S. Tannenbaum A. Angenent, S. and R.: Kikinis. On area preserving mappings of minimal distortion. *System Theory. Springer US*, pages 275–286, 2000.
[2] F. L. Bookstein. Principal warps - thin-plate splines and the decomposition of deformations. *Ieee Transactions on Pattern Analysis and Machine Intelligence*, 11(6):567–585, 1989.
[3] Lam K. C. Choi, P. T. and L. M.: Lui. Lash: Fast landmark aligned spherical harmonic parameterization for genus-0 closed brain surfaces. *SIAM Journal on Imaging Sciences*, 8(1):67–94, 2015.
[4] Meyer M. Desbrun, M. and P.: Alliez. Intrinsic parameterizations of surface meshes. *Computer Graphics Forum*, 21(3):209–218, 2002.
[5] T. J. Dolinsky, J. E. Nielsen, J. A. McCammon, and N. A. Baker. Pdb2pqr: an automated

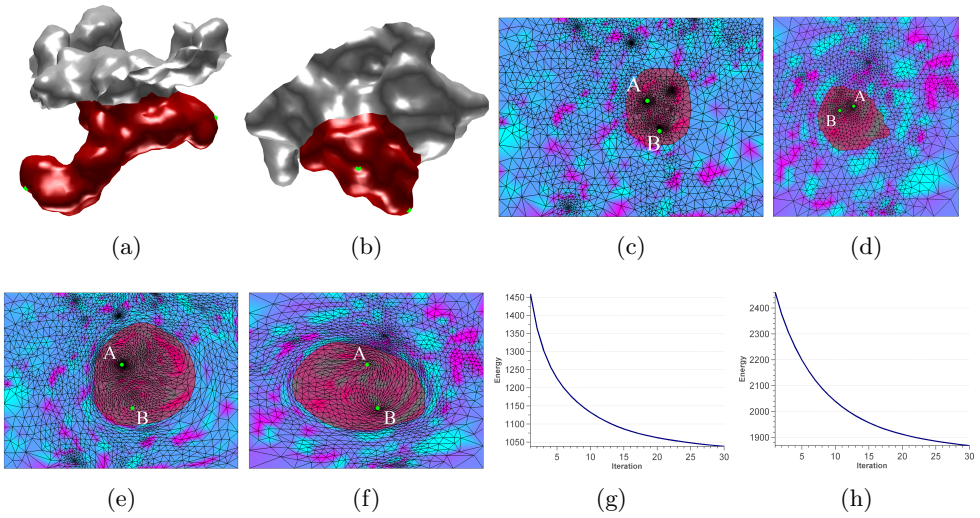

(a) (b) (c) (d)

(e) (f) (g) (h)

Fig. 6.12: (a) shows the selected region of Protein 4CS4. The red region is where we want to zoom-in on the 2D parameter domain. (b) shows the selected region of Protein 4D2I. The red region is where we want to zoom-in on the 2D parameter domain. (c) and (d) show the conformal parameterization of (a) and (b) respectively. Corresponding feature landmarks are labeled as green dots on the parameter domains. (e) shows the landmark-aligned optimized parameterization of (a). (f) shows the landmark-aligned optimized parameterization of (b). (g) and (h) show the energies versus iterations for (e) and (f) respectively.

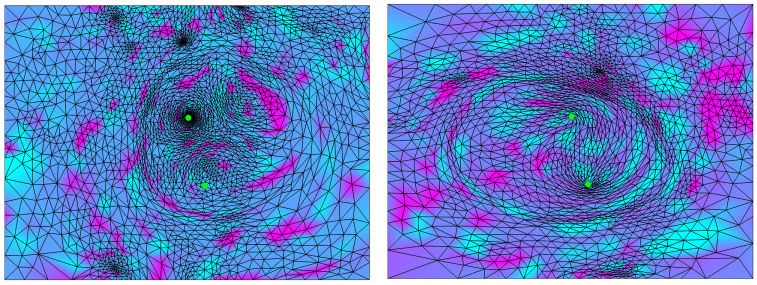

(a) (b)

Fig. 6.13: (a) and (b) shows the parameterized mesh of Figure 6.12(a) and (b) respectively, whose colormaps are given by the electostatic information.

pipeline for the setup of poissonboltzmann electrostatics calculations. *Nucleic acids research*, 32(2):656–667, 2004.

[6] A. Dominitz and A.: Tannenbaum. Texture mapping via optimal mass transport. *Visualization and Computer Graphics, IEEE Transactions on*, 16(3):419–433, 2010.

[7] Frederick P. Gardiner and Nikola Lakic. *Quasiconformal Teichmüller theory*. Mathematical surveys and monographs,. American Mathematical Society, 2000.

[8] Qiu A. Miller M. I. Glauns, J. and L.: Younes. Large deformation diffeomorphic metric curve

mapping. *International journal of computer vision*, 80(3):317–336, 2008.
[9] Vaillant M. Glauns, J. and M. I.: Miller. Landmark matching via large deformation diffeomorphisms on the sphere. *Journal of mathematical imaging and vision*, 20(1-2):179–200, 2004.
[10] X.F. Gu, Y. Wang, T.F. Chan, P.M. Thompson, and Yau S.T.:. Genus zero surface conformal mapping and its application to brain surface mapping. *IEEE Transaction on Medical Imaging*, 23(8):949–958, 2004.
[11] S. Haker, S. Angenent, A. Tannenbaum, R. Kikinis, and G. Sapiro. Conformal surface parameterization for texture mapping. *Ieee Transactions on Visualization and Computer Graphics*, 6(2):181–189, 2000.
[12] M. K. Hurdal and K. Stephenson. Discrete conformal methods for cortical brain flattening. *Neuroimage*, 45(1):S86–S98, 2009.
[13] A. Jacobson and O.: Sorkine. A cotangent laplacian for images as surfaces. *ACM Trans. Graph.*, 25(3):646–653, 2012.
[14] M. Jin, J. Kim, F. Luo, and X. Gu. Discrete surface ricci flow. *Visualization and Computer Graphics*, 14(5):1030–1043, 2008.
[15] M. Jin, J. H. Kim, F. Luo, and X. F. Gu. Discrete surface ricci flow. *Ieee Transactions on Visualization and Computer Graphics*, 14(5):1030–1043, 2008.
[16] S. C. Joshi and M. I.: Miller. Landmark matching via large deformation diffeomorphisms. *Journal of mathematical imaging and vision*, 9(8):1357–1370, 2000.
[17] Gu X. Lam, K. C. and L. M.: Lui. Genus-one surface registration via teichmller extremal mapping. *Medical Image Computing and Computer-Assisted InterventionMICCAI 2014. Springer International Publishing.*, pages 25–32, 2014.
[18] K.C. Lam and L.M. Lui. Landmark and intensity based registration with large deformations via quasi-conformal maps. *SIAM Journal on Imaging Sciences*, 7(4):2364–2392, 2014.
[19] Olli Lehto and K. I. Virtanen. *Quasiconformal mappings in the plane.* Die Grundlehren der mathematischen Wissenschaften in Einzeldarstellungen mit besonderer Berücksichtigung der Anwendungsgebiete. Springer, Berlin, Heidelberg, New York,, 2nd edition, 1973.
[20] Gu X. F. Lui, L. M. and S. T. : Yau. Convergence analysis of an iterative algorithm for teichmller maps via harmonic energy optimization. *Math. Comp.*, 2014.
[21] L. M. Lui, K. C. Lam, T. W. Wong, and X. F. Gu. Texture map and video compression using beltrami representation. *Siam Journal on Imaging Sciences*, 6(4):1880–1902, 2013.
[22] L. M. Lui, Y. L. Wang, T. F. Chan, and P. Thompson. Landmark constrained genus zero surface conformal mapping and its application to brain mapping research. *Applied Numerical Mathematics*, 57(5-7):847–858, 2007.
[23] L. M. Lui and C. : Wen. Geometric registration of high-genus surfaces. *SIAM Journal on Imaging Sciences*, 7(1):337–365, 2014.
[24] Lam K. C. Yau S. T. Lui, L. M. and X. : Gu. Teichmuller mapping (t-map) and its applications to landmark matching registration. *SIAM Journal on Imaging Sciences.*, 7(1):391–426, 2014.
[25] Thiruvenkadam S. R. Wang Y. Thompson P. M. Lui, L. M. and T. F: Chan. Optimized conformal surface registration with shape-based landmark matching. *SIAM J. Imaging Sciences*, 3(1):52–78, 2010.
[26] Thiruvenkadam S. Wang Y. Chan T. Lui, L. M. and P. : Thompson. Optimized conformal parameterization of cortical surfaces using shape based matching of landmark curves. *Medical Image Computing and Computer-Assisted InterventionMICCAI. Springer Berlin Heidelberg.*, pages 494–501, 2008.
[27] Petitjean S. Ray N. Lvy, B. and J.: Maillot. Least squares conformal maps for automatic texture atlas generation. *ACM Transactions on Graphics (TOG)*, 21(3):362–371, 2002.
[28] Tong Y. Alliez P. Mullen, P. and M.: Desbrun. Spectral conformal parameterization. *Computer Graphics Forum*, 27(5):1487–1494, 2008.
[29] Gu X. F. Ng, T. C. and L. M.: Lui. Teichmuller extremal map of multiply-connected domains using beltrami holomorphic flow. *J. Sci. Comput.*, 60:249–275, 2013.
[30] Richard Schoen and Shing-Tung Yau. *Lectures on differential geometry.* Conference proceedings and lecture notes in geometry and topology. International Press, Cambridge, MA, 1994.
[31] F. B. Sheinerman, R. Norel, and B. Honig. Electrostatic aspects of proteinprotein interactions. *Current opinion in structural biology*, 10(2):153–159, 2000.
[32] N. Sinha and S. J. Smith-Gill. Electrostatics in protein binding and function. *Current Protein and Peptide Science*, 3(6):601–614, 2002.
[33] D. Tosun, M. E. Rettmann, and J. L. Prince. Mapping techniques for aligning sulci across multiple brains. *Medical Image Analysis*, 8(3):295–309, 2004.
[34] M. Vaillant and J. : Glauns. Surface matching via currents. *Information Processing in Medical*

Imaging. Springer Berlin Heidelberg, pages 381–392, 2005.

[35] Kim J. Luo F. Hu S. M. Yang, Y. L. and X. Gu. Optimal surface parameterization using inverse curvature map. *Visualization and Computer Graphics, IEEE Transactions on*, 14(5):1054–1066, 2010.

[36] Lui L. M. Shi L. Wang D. Chu W. C. Cheng J. C. ... Zeng, W. and X Gu. Shape analysis of vestibular systems in adolescent idiopathic scoliosis using geodesic spectra. *Medical Image Computing and Computer-Assisted InterventionMICCAI. Springer Berlin Heidelberg*, pages 538–546, 2010.

[37] W. Zeng and X. D.: Gu. Registration for 3d surfaces with large deformations using quasi-conformal curvature flow. *Computer Vision and Pattern Recognition (CVPR), 2011 IEEE Conference on.*, pages 2457–2464, 2011.

[38] Su Z. Gu X. D. Kaufman A. Sun J. Gao J. Zhao, X. and F.: Luo. Area-preservation mapping using optimal mass transport. *Visualization and Computer Graphics, IEEE Transactions on*, pages 2838–2847, 2013.

[39] Hu J. Gu X. Zou, G. and J.: Hua. Area-preservation surface flatttening using lie advection. *Medical Image Computing and Computer-Assisted InterventionMICCAI, Springer Berlin Heidelberg*, pages 335–342, 2011.